Quantifying Effective Built-in Temperature Difference for Decades-Old Jointed Plain Concrete Pavements in Eastern Washington State

Zhao Chen[1], Somayeh Nassiri[2], Jeff Uhlmeyer[3]

Abstract

Fifteen Portland cement concrete (PCC) slabs from four Jointed Plain Concrete Pavement (JPCP) sections in the Long-Term Pavement Program (LTPP) located in eastern Washington State were studied in this paper. Dipstick-measured transverse deflection profile along with temperature measurements across slabs' depths collected during falling weight deflectometer (FWD) testing were used in the study. The youngest section in the study was 24 years old at the time of testing. The objective was to characterize the total effective linear temperature difference (TELTD) and the effective built-in temperature difference (EBITD) in the slabs. EBITD is a temperature differential representing the combined effects of construction built-in, as well as long-term drying shrinkage, and creep equivalent temperature differences. Using ISLAB2000, several iterations were run for each slab to identify the TELTDs that would produce slab curvatures close to those measured in the field. For validation purposes, the found TELTDs were used in Westergaard's closed-form solution for deflections in the transverse direction. Transverse profiles predicted by ISLAB2000 and Westergaard equations matched well. EBITD, was then obtained by simply subtracting the in-field measured temperature differential from TELTD. Variations of EBITDs were found among the four sections, ranging from +31 to -120 °C (55 to -215 °F). Multiple factors, such as structural features, material properties, construction conditions, and climatic conditions, were identified as influential for the predicted EBITDs.

Introduction

Shape of the Portland cement concrete (PCC) slabs in concrete pavements is affected by the magnitude and signage of transient temperature differentials between the top and bottom of the slab ($\Delta T_{tran} = T_{top} - T_{bottom}$). In the presence of $\Delta T_{tran} > 0$ during the day, the slab is warmer at the top relative to the bottom and thereby expands more at the surface–this shape is referred to as downward curling. In this case, the slab loses contact and support from the underlayer in the middle portion. The self-weight of the slab and other restrictions, such as the aggregate interlock and load transfer efficiency (LTE) devices along the joints and the friction with the base layer resist the curling movements and result in the development of tensile stresses in the middle portion, initiating from the bottom. It is due to accumulation of these stresses, especially when enhanced by wheel load applications in the unsupported middle portion, that bottom-up fatigue cracking manifest in the slab. In the presence of $\Delta T_{tran} < 0$ (typically during the night), the top portion of the slab is cooler compared to the bottom portion and contracts more resulting in the slab edges to lift up and the middle portion to sink in the base layer (this situation is referred to as an upward curvature). In this case, the slab is unsupported along the edges and can crack from the top at mid-panel,

[1] PhD student, Washington State University (WSU), zhao.chen@wsu.edu, Phone: (575) 621-533.
[2] Assistant Professor, WSU, snassiri@wsu.edu, Tel: (509) 335-7455, Fax: (509) 335-7632.
[3] State Pavement Engineer, WSDOT, uhlmeyJ@wsdot.wa.gov, Tel: (360) 709-5485, Fax: (360) 709-5588

especially when axle loads are applied along the unsupported edges. The curling behavior of the slab in response to ΔT_{tran} was known to researchers at early ages of design of slab on grade. Westergaard (1927) developed a closed-form solution for estimating the tensile stresses that develop in the slab due to a linear temperature differential as defined above.

However, it was found only in the past two decades that other factors play roles in forming the slab's long-term curvature, as the slab was not found to be flat when $\Delta T = 0$ (Armaghani et al. 1987, Eisenmann and Leykauf 1990, Yu et al. 1998). One of these factors is the $\Delta T_{built-in}$, which is the ΔT that locks into the slab at the zero-stress time (TZ). TZ is typically reached within the early hours of construction, depending on climatic conditions and other factors, and it is the point in time when the PCC is still too fresh to develop any tensile stresses. It is past this point in time that the fresh PCC slab reaches adequate rigidness to start to curl in response to ΔT_{tran} (Nassiri et al. 2014). Warm and sunny days are typically preferred for construction, resulting in $\Delta T_{built-in} < 0$, which cancels the downward curling due to positive ΔT_{tran} and adds to the upward curling due to negative ΔT_{tran}. In this case, the slab curls upward for most of time or the whole time, if the $\Delta T_{built-in}$ is large enough (Yu et al. 1998).

In addition to $\Delta T_{built-in}$, differential drying shrinkage occurring at the upper 51-mm (2 inch) portion of the slab results in both seasonal and permanent upward curvature–typically referred to as warping (Janssen 1987, Eisenmann and Leykauf 1990, Rao and Roesler 2005). Besides the reversible seasonal expansion in wetter months of the year, a portion of the drying shrinkage does not reverse and the slab remains shrunk permanently. Research has shown that it takes about 4-5 years for the slab to assume permanent warping due ultimate drying shrinkage, depending on climatic conditions (Burnham and Kouba 2001) To be able to incorporate this effect of the warping due to the drying shrinkage into Westergaard's solutions, another equivalent ΔT that produces the same upward curvature as drying shrinkage, hereafter referred to as ΔT_{shri}, was introduced (Eisenmann and Leykauf 1990).

Finally, slab's self-weight and restraints at joints create a constant loading condition for the slab, resulting in relaxation due to creep. It has been theorized that creep contributes to partial recovery of the slab curvature due to $\Delta T_{built-in}$ and ΔT_{shri} (Yu and Darter 2004, Rao and Roesler 2005, Kim et al. 2010). Similar to drying shrinkage, creep needs to be defined in terms of ΔT to be incorporated in Westergaard's solution (ΔT_{creep}).

The combined effect of the above environmental factors that affect the slab curvature can be represented by one linear ΔT called the total effective linear temperature difference (TELTD), and can be defined as shown in Equation 1. Slab curling and warping due to the accumulated effects of $\Delta T_{built-in}$, ΔT_{shri} and ΔT_{creep} will be referred to as the effective built-in temperature difference (EBITD) (Rao and Roesler 2005). It can be seen in Equation 1 that TELTD for a slab is equal to the sum of its EBITD and ΔT_{tran}.

$$\mathrm{TELTD} = \Delta T_{tran} + \underbrace{\Delta T_{built-in} + \Delta T_{shri} - \Delta T_{creep}}_{\mathrm{EBITD}} \qquad \text{Eq. 1}$$

EBITD needs to be characterized because it is directly related to the cumulative tensile stresses that ultimately result in fatigue cracking in the slab. Insufficient considerations for EBITD in the design can result in misjudging the fatigue life and thereby the slab thickness design. While critical to the performance prediction process, due to its complex, gradual and continuous stabilization over the years, EBITD is difficult to estimate. Part of the challenge is that limited field data is available on the actual EBITD for in-service pavements. Rao et al. (2001) estimated EBITDs based on diagonal surface profile measurements for jointed plain concrete pavement (JPCP) s in Minnesota and Arizona. EBITDs for the section in Mankato, Minnesota were found to be -7.3˚C (-13.1˚F) at set time, -27.4˚C (-49.2˚F) at 40 days after paving, and -21.9˚C (-39.4˚F) at 2 years after paving. EBITDs for the sections in Phoenix, Arizona ranged from -11.8 to -27.4˚C (-23.1 to -41.5˚F) at 3 days after paving and from -20 to -29.1˚C (-36 to -52.4˚F) at 40 days after paving. In another study, using slab deflection measurements at corners and mid-slab edges for JPCPs in Palmdale, California at early ages (within one year after paving), Rao and Roesler (2005) predicted EBITD of -20 to -35˚C (-36 to -63˚F) for JPCP sections with low restraints (no dowels or tied concrete shoulder) and EBITD of 0 to -20˚C (-36˚F) for sections with high restraints (widened lane and tied concrete shoulders with dowels). Rao et al. (2011) used the Mechanistic-Empirical Pavement Design Guide (MEPDG) software for 300 JPCP sections across the country with varying EBITD values. The MEPDG-predicted fatigue cracking were then compared to field distress data to identify the EBITD that resulted in the least error in distress predictions for each section. A statistical model was developed to correlate the select EBITD values to material properties, structural features, climate parameters, and geographical locations. In 2012, Nassiri and Vandenbossche put forward a procedure for stablishing EBITD through estimated early-age $\Delta T_{built\text{-}in}$ [ranging from 5.4 to -21.6 ˚C (9.7 to 38.9 ˚F)] for four different JPCP sections in Pennsylvania. Additionally, the effect of long-term ΔT_{shri} and ΔT_{creep} was incorporated in the procedure based on long-term in-situ axial strain measurements in another test section in Pennsylvania and the Minnesota Department of Transportation's test road facility (MnRoad). The developed procedure was used to predict the five-year ΔT_{shri} for different climatic regions in Pennsylvania ranging from -5 to -30 ˚C (-9 to -54 ˚F).

The present study puts forward a procedure, where the slab transverse profile data already being collected as part of the Long Term Pavement Performance Program (LTPP) can be used to estimate EBITD. During the study, it was found that slab temperature profile is not measured as part of the profile measurements for the LTPP program. To compensate for this limitation, the profile measurements taken on the day of falling weight deflectometer (FWD) testing were used in the study, which limited the number of test sections to four. The four LTPP sections were all more than 24 years old at the time of study. All four sections are composed of unbound base layers with no dowels installed along transverse joints at the time of construction. ISLAB2000, a commercially available finite element method (FEM)-based software was used to predict TBITD, and EBITD by subtracting the ΔT_{tran} measured during FWD testing from TBITD. The possible effect of various material, environment, and construction-related factors on the predicted EBITD was also investigated.

Overview of Test Sections

Location and Construction. Four JPCP sections in the LTPP program located in eastern Washington State were able to be included in this study. The Strategic Highway Research program (SHRP) Identification number and the geographical locations of these sections are shown in Figure 1. The highway route number, average yearly equivalent single axle load (ESAL)s, construction and maintenance history for each section are provided in Table 1. As seen in Table 1, the PCC slabs were restored for Sections 3013 and 7409 by diamond grinding in 2010 and 2011, which limited the data used in the study to those collected prior to the grinding events. The average yearly kESALs for Section 3013 is much lower than the other sections (62.8 kESAL compared to around 541, 626 and 493 kESAL). All four sections were designed for a 50-year design life as per

Washington Department of Transportation (WSDOT)'s design requirements. According to LTPP's distress records for the sections, three of the sections are in good conditions, while Section 7409 shows low and medium severity fatigue cracking. All sections are 152.4 m (499.9 ft) long and are compo sed of two lanes in each traffic direction. The data was collected in the outer lane, which is 3.66 m (12 ft) wide with various joint spacing among the sections.

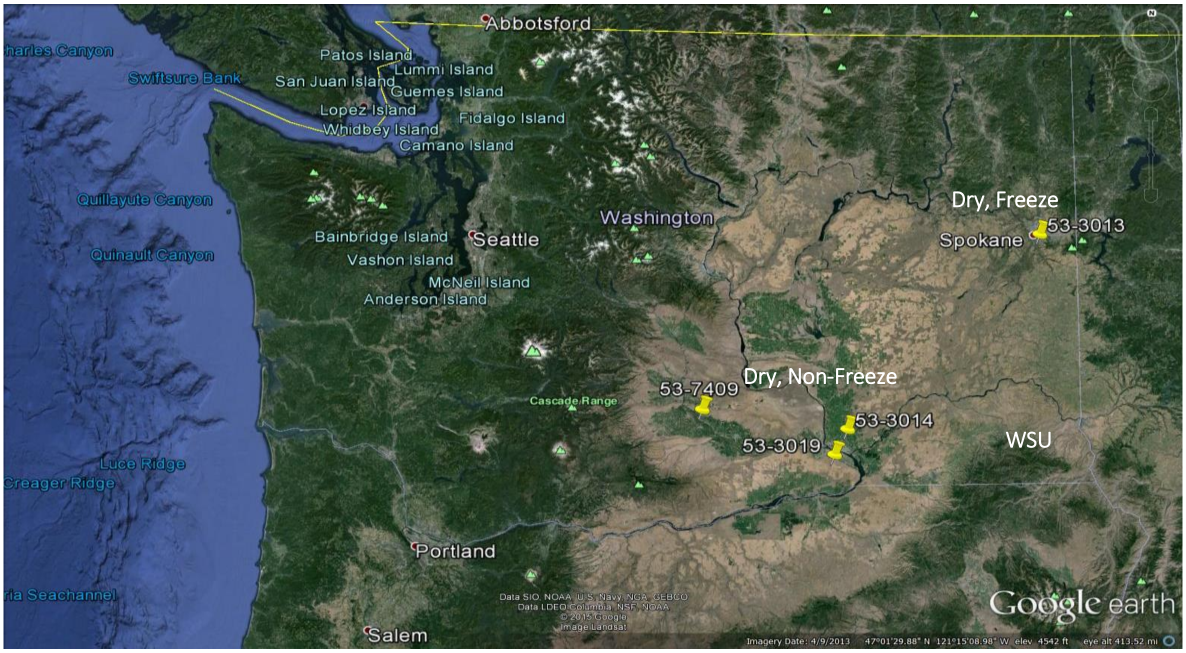

Figure 1. Geographical Locations of the Studied JPCP Sections in Washington State (47°01'29.88" N 121°15'08.98" W. **Google Earth**. April 9, 2013. September 21, 2015)

Table 1. Location Information and Construction and Maintenance History of the Studied Sections

SHRP ID	**Route Direction**	**County, State**	**Average Yearly KESALs**	**Construction Date**	**Traffic Open Date**	**Maintenance & Rehabilitation Event**
53-3013	U.S. 195 North Bound	Spokane, WA	62.8	10/1/1970	2/1/1971	Grinding Surface; Joint Load Transfer Restoration on 4/1/2010
53-3014	U.S. 395 North Bound	Franklin, WA	541.0	4/1/1986	4/1/1987	None
53-3019	Interstate 82 East Bound	Benton, WA	625.5	4/1/1986	8/1/1986	None
53-7409	Interstate 82 East Bound	Yakima, WA	493.3	5/1/1981	5/1/1981	Shoulder Restoration; Grinding Surface; Joint Load Transfer Restoration on 8/4/2011

Structure and Material. Thickness and material type for each layer for the four sections are schematically illustrated in Figure 2. As seen in the figure, the surface PCC layer varies between 208 mm (8.2 in.) and 264.2 mm (10.4 in.) among the four sections. The base layer material type for all sections is unbound made of crushed gravel, except for Section 3014, which is made of a soil-aggregate mixture. The mechanical properties and the coefficient of thermal expansion (CTE) of the PCC for the four sections are shown in Table 2. Also provided in Table 2 are the modulus of elasticity of the PCC layer (E_c), the base layer (E_b), and the subgrade k-value. The backcalculated values were obtained from the "Deflection-Backcal Data" of the LTPP database.

The LTPP file contains backcalculated layers' moduli by the Best-fit method. The moduli presented in Table 2 are static values, which are 80 and 50 percent of the dynamic E_c and k-value, respectively (ASSHTO 1993). PCC mix designs, obtained from the "PCC-Mixture Design (inventory)" of the Material Section in the LTPP database, are also summarized in Table 2. All sections had random transverse joint spacing as provided in Table 3. Transverse joint LTE values are available in the LTPP database based on FWD tests at joint locations and are provided in Table 3 as well. Note that for each section, only those slabs included in the study (as discussed in the succeeding sections) are listed in Table 3.

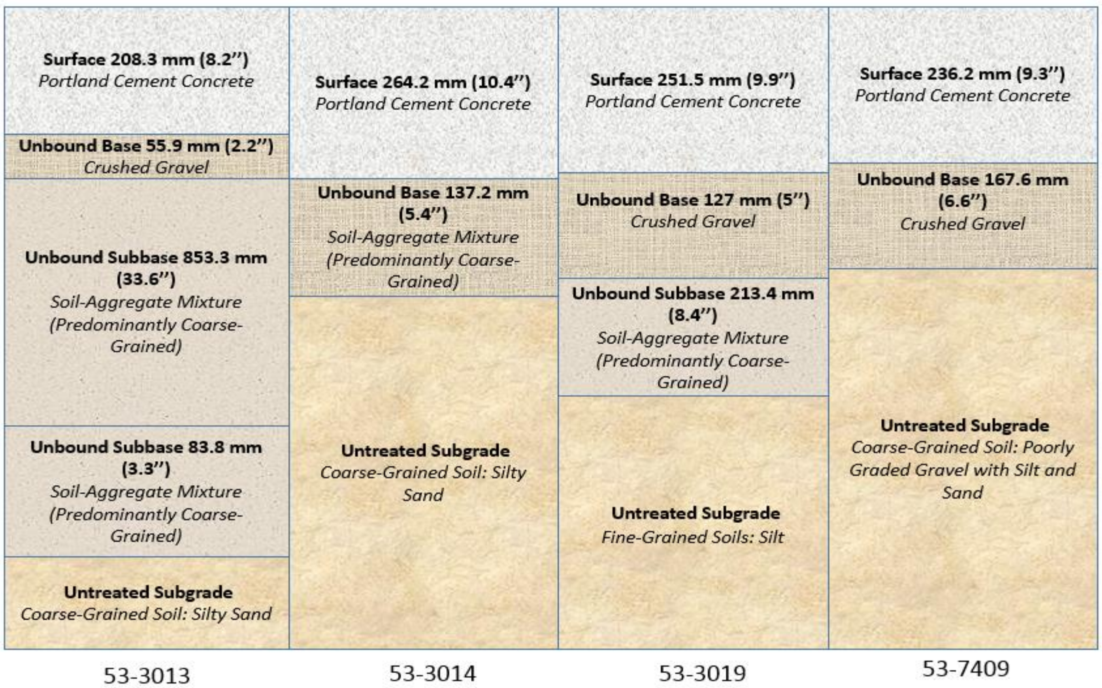

Figure 2. Schematic Cross Sections of Studied Sections

Transverse Profile and Slab Temperature Date. Slab transverse profile measured using a Dipstick profiler accompanied by measurements of temperature throughout the slabs' depths are required for this study. There are total of 22 LTPP JPCP sections in Washington, however, as mentioned previously, slab temperature is not measured at the time of profile measurement as part of the LTPP data collection. To resolve this problem, the day and time when profile measurements were taken were matched with FWD tests, resulting in the four select JPCP sections. Test dates and times for the four sections are shown in Table 4. As seen in the Table 4, the times of profile and slab temperature measurements are within 5-20 minutes of each other. Slab temperature is not expected to vary considerably in this time span.

Figure 3 (a) and (b) show examples of the transverse profiles measured for all the slabs on Section 3014 on 6/14/2005. As seen in Figure 3 (a), transverse profiles were measured at approximately every 15 m (50 ft) throughout the section (falling at about mid-slab for some slabs and closer to the joints for others).Transverse profiles needed to be first corrected to remove the transverse slope as shown in Figure 3 (b). Also, apparent in Figure 3 (a) are ruts in the wheelpaths, created by studded tires used during winter months in the Pacific Northwest. The data points that create the distinct valleys in the wheelpaths in each profile were removed from the profile. The effect of studded tires' wander to areas other than the wheelpaths on slab profile is assumed to be negligible in this study. A second-order polynomial was fitted through the remaining data points for each slab [see Figure 3 (b)]

Table 2. Mechanical Properties and Mix Design

SHRP ID		**53-3013**	**53-3014**	**53-3019**	**53-7409**
Cement Weight - kg/m^3 (lb/yd^3)		335 (565)	335 (565)	335 (565)	335 (565)
Water Weight - kg/m^3 (lb/yd^3)		148.8 (251)	112.1 (189)	115 (194)	145.3 (245)
Water/Cement Ratio		0.44	0.33	0.34	0.43
Cement Type		Type II	Type II	Type II	Type II
Entrained Air Mean - %		4.9	6.8	4.3	5.8
Slump - mm (in)		71.1 (2.8)	58.4 (2.3)	27.9 (1.1)	45.7 (1.8)
Density - kg/m^3 (pcf)		2419.02 (151)	2443.0 (152.5)	2451.06 (153)	2338.92 (146)
Coarse Aggregate Weight - kg/m^3 (lb/yd^3)		1221.6 (2060)	1235.2 (2083)	1221.6 (2060)	1221.6 (2060)
Fine Aggregate Weight - kg/m^3 (lb/yd^3)		729.4 (1230)	673.1 (1135)	729.4 (1230)	729.4 (1230)
PCC Layer	**E_c - kPa (psi)**	4.59E+07 (6.66E+06)	2.27E+07 (3.29E+06)	2.67E+7 (3.87E+6)	2.66E+07 (3.85E+6)
	Poisson's Ratio	0.14	0.19	0.145	0.175
	Density - kg/m^3 (pcf)	2418.8 (151.0)	2442.8 (152.5)	2450.8 (153)	2338.7 (146)
	CTE - mm/mm/°C (in/in/°F)	9.5E-6 (5.27E-6)	7.71E-6 (4.29E-6)	8.03E-6 (4.46E-6)	7.32E-6 (4.07E-6)
Base Layer	**E_b - kPa (psi)**	2.63E+5 (3.81E+4)	9.1E+4 （1.32E+4)	1.52E+5 (2.21E+4)	1.52E+5 (2.20E+4)
	Poisson's Ratio	0.2	0.2	0.2	0.2
	Density - kg/m^3 (pcf)	2226.8 (139.0)	2136.0 (133.3)	2194.7 (137.0)	2285.5 (142.7)
Subgrade	**k-value - MPa/m (pci)**	20.25 (75)	15.39 (57)	10.8 (40)	6.35 (23.5)

Table 3. Joint Spacing and LTE for the Studied Slabs

SHRP ID	**Slab No.**	**Joint Spacing - m (ft)**	**LTE - %**
53-3013	1	5.49 (18)	89
53-3013	2	5.49 (18)	92
53-3013	3	5.49 (18)	92
53-3014	1	3.96 (13)	95
53-3014	2	3.96 (13)	95
53-3014	3	3.05 (10)	96
53-3019	1	4.27 (14)	56
53-3019	2	4.27 (14)	92
53-3019	3	3.96 (13)	85
53-3019	4	3.96 (13)	63
53-3019	5	3.96 (13)	85
53-7409	1	3.96 (13)	81
53-7409	2	4.27 (14)	88
53-7409	3	4.27 (14)	90
53-7409	4	4.27 (14)	92

Table 4. Tests' Dates and Times

SHRP ID	Test Date	Transverse Profile Measuring Time	Pavement Temperature Profile Measuring Time during FWD Tests
53-3013	8/20/2003	2:23 p.m.	2:04 p.m.
53-3014	6/14/2005	8:44 a.m.	9:03 a.m.
53-3019	6/13/2005	10:55 a.m.	10:50 a.m.
53-7409	6/9/2005	10:38 a.m.	10:55 a.m.

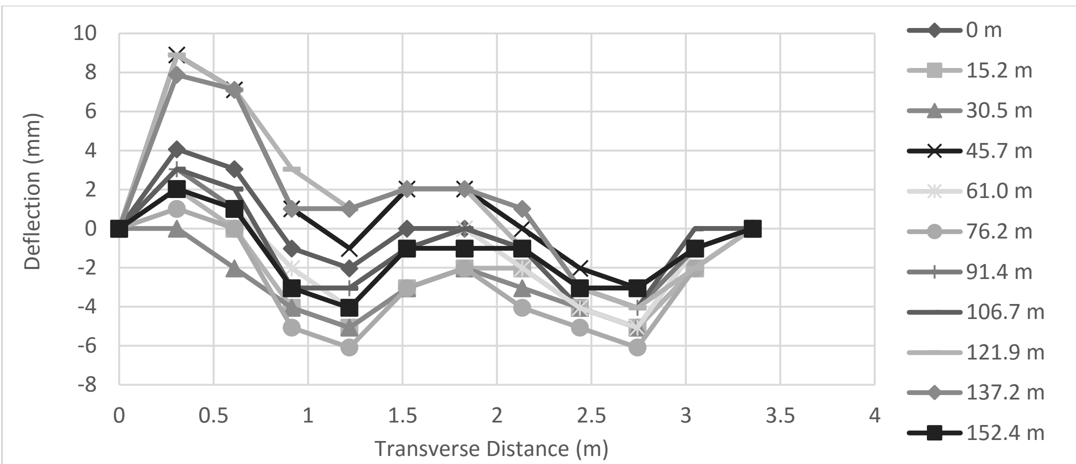

(a)

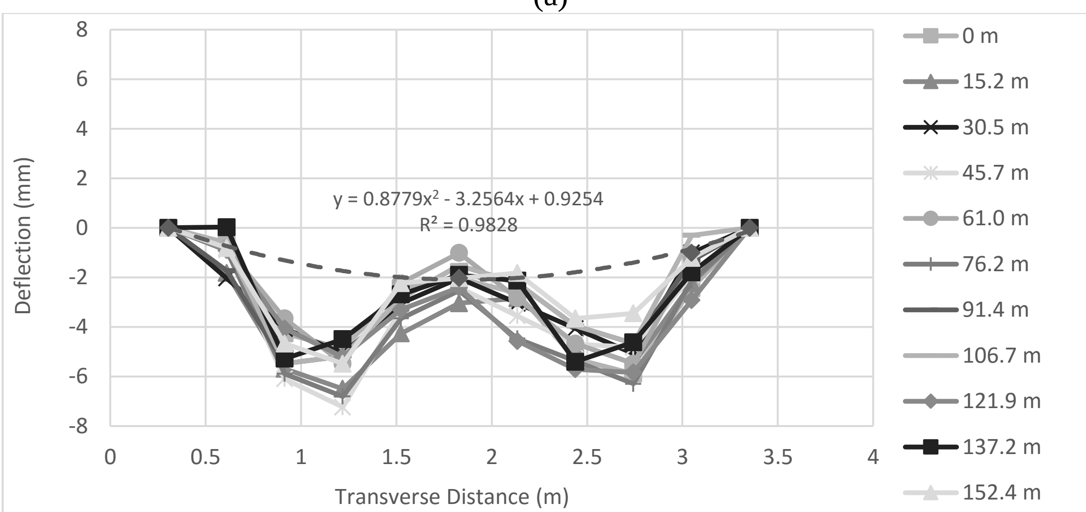

(b)

Figure 3. Section 3014 - 8:44 a.m. 6/14/2005: (a) Transverse Profiles (b) Transverse Profiles after Subtracting Slope and with a polynomial fitted for Slab 1 at 15.2 m.

Finite Element Model. ISLAB2000 was used to predict TBITDs for the slabs in the four sections under study. FEM models were developed for the slabs in each of the four sections in accordance with the structural features presented previously in Figure 2. The subgrade support was modeled as Winkler foundation. For each slab under study, a nine-slab model as shown in Figure 4 was constructed in ISLAB2000. Material properties for each layer was defined as provided in Table 2-note that dynamic moduli were used for this analysis. Transverse joint LTE and spacing was defined as presented in Table 3. FWD tests were only conducted at one transverse joint on each slab and the LTE for the other joint was assumed to be the same as the test joint. All four sections have Asphalt Concrete (AC) outer shoulders and the truck lane is tied to the inner lane with tie bars. The longitudinal LTE for all slabs was assumed to be 20% for the joints with the AC shoulder and 70% for the joints with the inner lane according to the recommendations found in the (MEPDG documentation (ARA 2004).

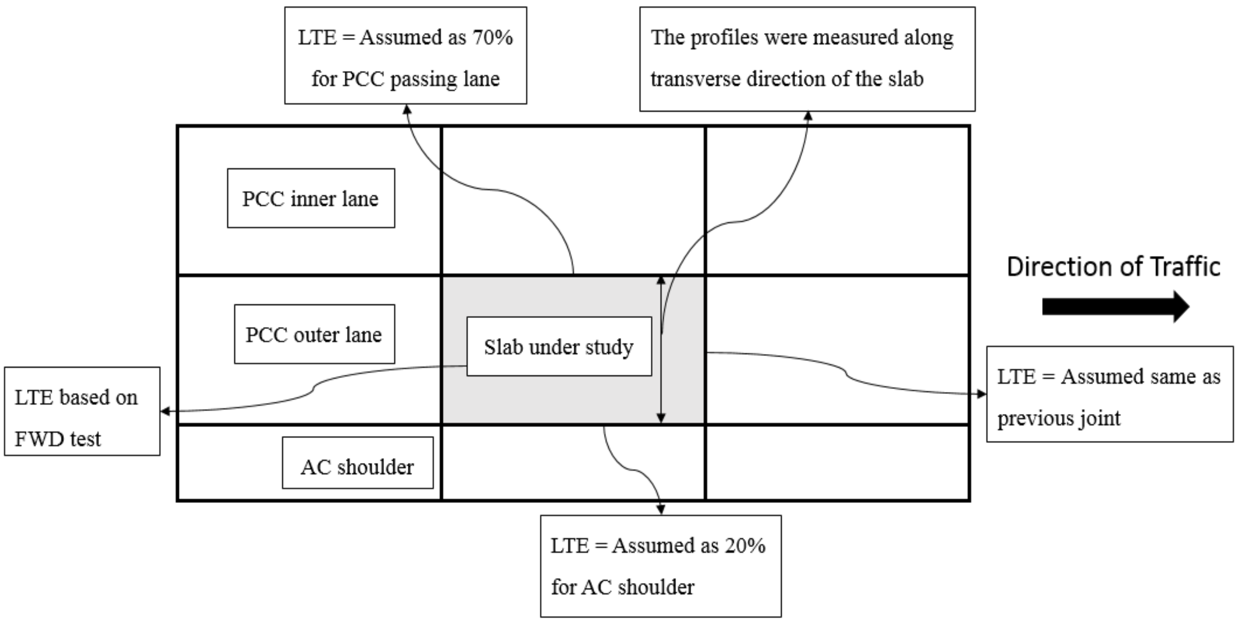

Figure 4 Layout of ISLAB2000 Model

First, to ensure that the average backcalculated layer moduli for each pavement section can be used for all slabs within the section, FWD tests was simulated for each slab using ISLAB2000. FWD tests conducted at mid-slabs were used for this purpose and the deflection measured under the load plate – most representative of the slab deflection – was used for validation. This procedure resulted in limiting the number of slabs that can be used in each section to those where the FWD tests were conducted-mostly every other slab but in some cases every third slab was tested. For each FWD testing, three load levels of 40.0 kN (9 kips), 53.4 kN (12 kips), and 71.2 kN (16 kips) were targeted, and each load level was dropped four times (Schmalzer 2006). The average load of four drops for each level were used in the models. The deflections at the center of the load plate were compared with those predicted by ISLAB2000 for all three load levels (see Figure 5). A total of 15 slabs that resulted in less than 15 percent error for the predicted slab deflections were selected for the TBITD study.

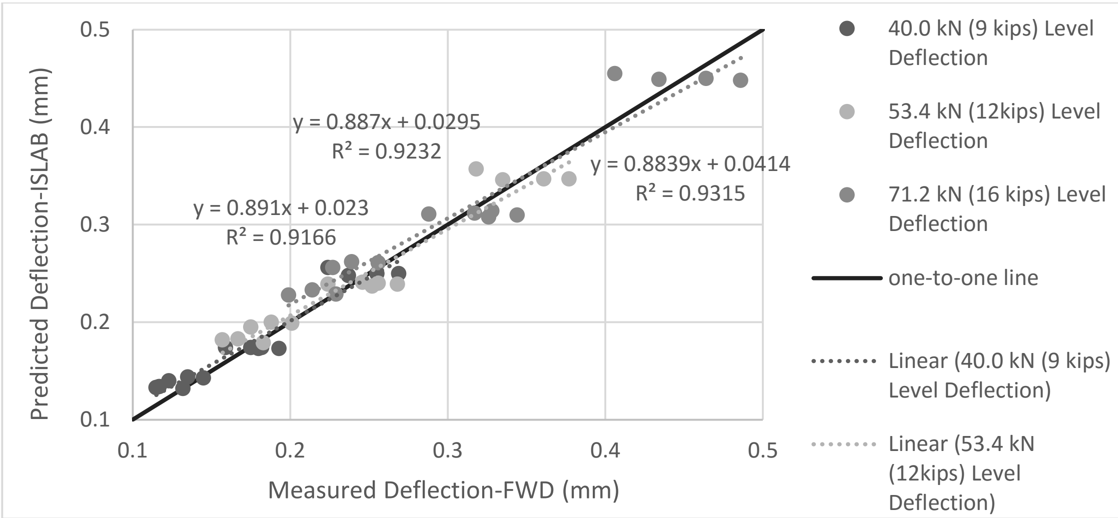

Figure 5. ISLAB Predicted Deflection versus FWD Measured Deflection

Predicting TBITD. The select models were modified to use the static moduli for each layer. After this modification, to predict TBITD for each slab, a linear ΔT was defined in ISLAB2000 starting at zero. This value for ΔT was then changed in increments of ±1.1 °C (±2 °F) to find the best fit between the predicted and measured slab profiles. In comparing the predicted and measured profiles, two indicators were used, 1- The predicted deferential deflection between the middle and the edge of the slab (δ_{mid}), and 2- The slab curvature in the transverse direction (ε_{trans}) obtained by taking the second derivative of the transverse deflection profile. ΔT that resulted in the minimum error between the predicted and measured δ_{mid} and ε_{trans} was found to be TBITD for the slab. As can been seen in Figure 6, the δ_{mid} and ε_{trans} predicted by FEM match well with the measured ones (less than one percent error).

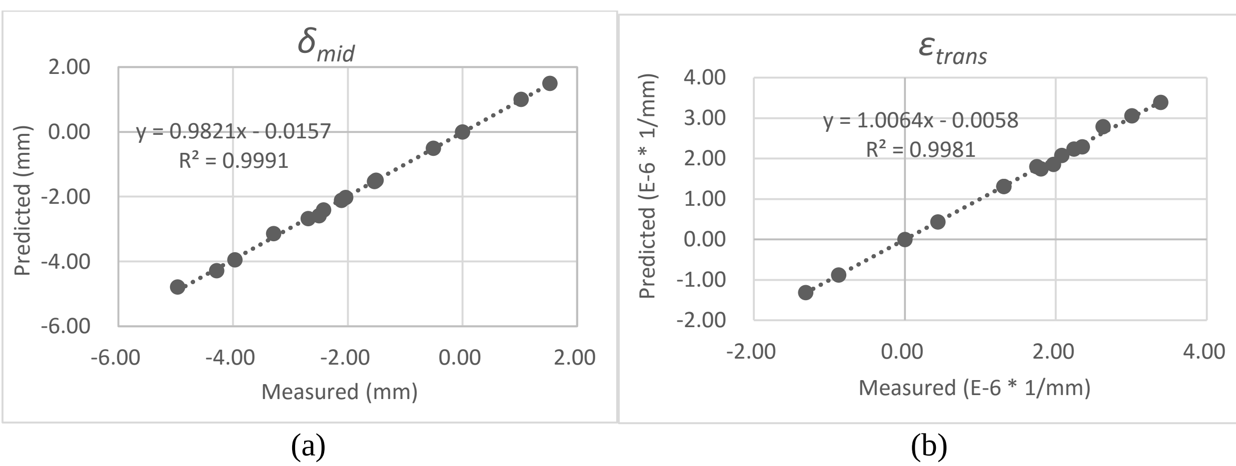

Figure 6. ISALB2000 Predicted versus Measured (a) δ_{mid} and (b) ε_{trans}.

Comparison to closed-form solutions. To validate the FEM predictions for TBITD, the obtained TBITDs were used to generate the slab transverse deflection profile using Westergaard's solution to compare with the ISLAB-predicted profiles. Westergaard's equations for computing slab's deflections along the transvers centerline due to a linear temperature difference are as follows (Westergaard 1927):

$$\delta_t = -\delta_0 \frac{2\,cos\lambda\,cosh\lambda}{sin2\lambda+sinh2\lambda}\left[(-tan\lambda + tanh\lambda)cos\frac{y}{l\sqrt{2}}cosh\frac{y}{l\sqrt{2}} + (tan\lambda + tanh\lambda)sin\frac{y}{l\sqrt{2}}sinh\frac{y}{l\sqrt{2}}\right] \quad \text{Eq.2}$$

Where:

$$\lambda = \frac{b}{l\sqrt{8}}$$

$$l = \sqrt[4]{\frac{Eh^3}{12(1-v^2)k}}$$

$$\delta_0 = \frac{l^2(1+v)\alpha t}{h}$$

E = Modulus of elasticity of the slab, ν = PCC Poisson's ratio. k = modulus of subgrade reaction. α = Coefficient of thermal expansion of concrete. h = slab thickness. t = temperature difference of the slab top from bottom. b = slab width. y = distance along the transverse line of the slab.

The comparisons of transverse profiles generated by ISLAB2000 versus those obtained using Westergaard equations for the four sections are shown in Figure 7 (a) through (d). It can be seen that the profiles by FEM match well with the ones by Westergaard equations.

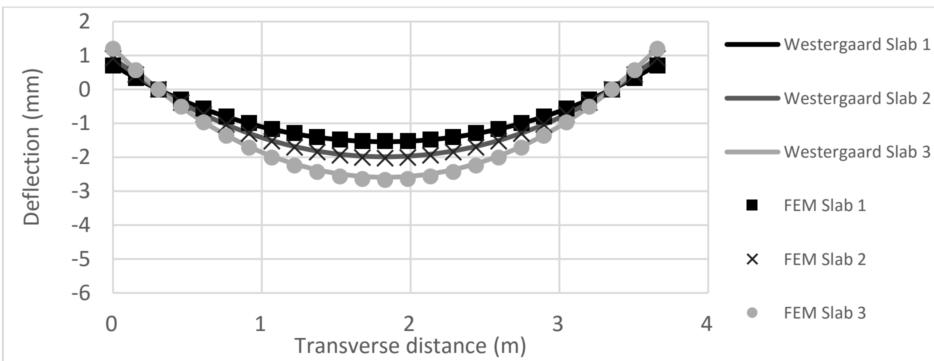

(a)

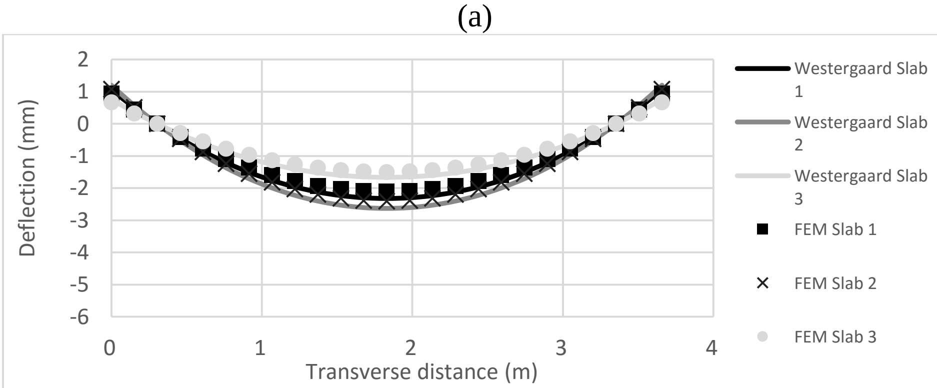

(b)

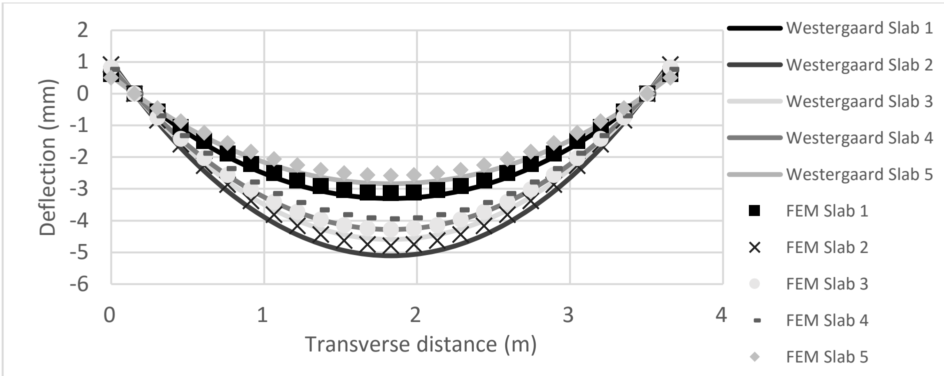

(c)

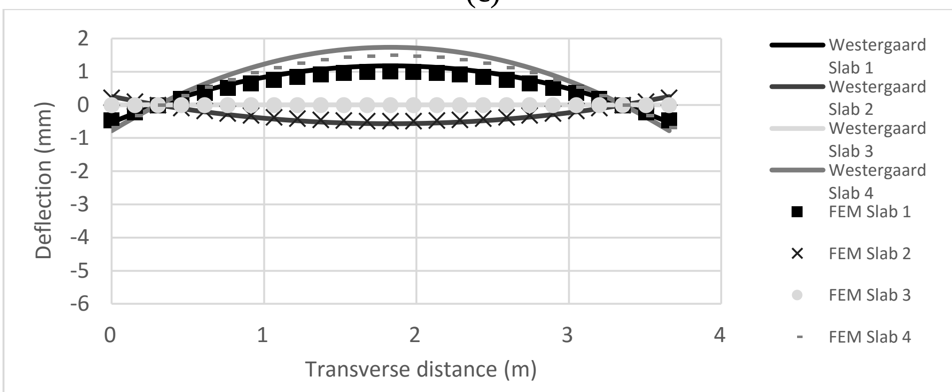

(d)

Figure 7. Predicted Transverse Profiles Comparisons of (a) Section 53-3013, (b) Section 53-3014, (c) Section 53-3019, (d) Section 53-7409.

Quantifying EBITD. As shown previously in Equation 1, EBITD is equal to TBITD subtracted by ΔT_{tran}. The measured temperature profiles for all the sections at the time of FWD testing are shown in Figure 8. As seen in the figure, the temperature distribution across the slabs were nonlinear. To consider the effect of nonlinearity of temperature across the slab, the concept of equivalent linear temperature difference was used. In this method, temperature-moment (TM) is used to quantify the effects of both linear and nonlinear temperature distribution throughout a PCC slab. If the TM of a nonlinear ΔT is equal to that of a linear ΔT, the two ΔT are treated as equivalent in affecting the slab curling (Janssen and Snyder 2000). The measured equivalent ΔT_{tran} was subtracted from the TBITD to obtain the EBITD for each slab. The TBITD, equivalent linear ΔT_{tran}, and EBITD of each slab are tabulated in Table 5.

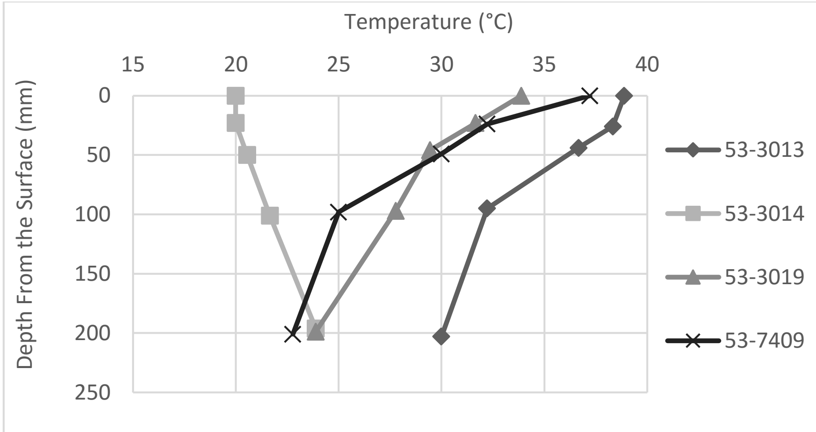

Figure 8. Temperature Profiles for all the Sections measured during FWD tests

Table 5. TBITD and EBITD for Each Slab

SHRP ID	Slab No.	TBITD- °C (°F)	ΔT_{tran}- °C (°F)	EBITD- °C (°F)
53-3013	1	-31 (-56)	9 (16)	-40 (-72)
53-3013	2	-40 (-72)	9 (16)	-49 (-88)
53-3013	3	-52 (-94)	9 (16)	-61 (-110)
53-3014	1	-67 (-120)	-5 (-9)	-62 (-111)
53-3014	2	-76 (-136)	-5 (-9)	-71 (-127)
53-3014	3	-48 (-86)	-5 (-9)	-43 (-77)
53-3019	1	-71 (-128)	10 (18)	-81 (-145)
53-3019	2	-110 (-198)	10 (18)	-120 (-215)
53-3019	3	-99 (-178)	10 (18)	-108 (-195)
53-3019	4	-92 (-166)	10 (18)	-102 (-183)
53-3019	5	-61 (-110)	10 (18)	-71 (-127)
53-7409	1	30 (54)	14 (25)	16 (29)
53-7409	2	-14 (-26)	14 (25)	-28 (-51)
53-7409	3	0 (0)	14 (25)	-14 (-25)
53-7409	4	44 (80)	14 (25)	31 (55)

Discussion of Results

From Table 4, it can been seen that the slabs in Section 3019 had the greatest negative EBITDs that range from -71 to -120 ˚C (-127 to -215 ˚F) (large upward curvature); the EBITDs of Section 3013 are around -50 ˚C (-90 ˚F); the EBITDs of Section 3014 are around -60 ˚C (-108 ˚F); Section 7409 shows both positive and negative EBITDs and these values are relatively small compared to the other three sections (close to a flat slab condition).

As discussed previously, EBITD depends on the combined effect of construction built-in curl, drying shrinkage, and PCC creep. The potential effect of different factors such as PCC mix design, structural features, and the climatic conditions on EBITD need to be investigated to understand the different EBITD values obtained for the four sections.

Structural Features. Restraints such as friction with the base layer, slab self-weight, and high LTE can prevent the slab from curling and warping. As shown earlier in Figure 2, all four sections have unbound base layers, so the interactions between PCC and base layer of the sections can be considered similar. Thinner slabs tend to curl/warp more freely because of less self-weight restraint. From Figure 2, Sections 3013 and 7409 have the thinnest slabs [208.3 mm (8.2 in) and 236.2 mm (9.3 in), respectively] compared to the other two sections [264.2 mm (10.4 in) and 251.5 mm (9.9in)]. However, they have lower EBITDs; also, slabs with lower density should result in more curl/warp due to less restraint and more creep. The densities of these sections are similar [around 2435 kg/m^3 (152 pcf)] except Section 7409, which has lowest density [2339 kg/m^3 (146 pcf)]. Nevertheless, it has lowest EBITDs. The variations in slab thickness and density among the four section are minimal, and perhaps not the differentiating factors among the sections' EBITD. Thus, other structural and environmental factors are required to explain this behavior. In terms of LTE, none of the sections have dowels installed along the transverse joints between the construction date and the test dates, therefore the restraints from the joints depend on aggregate interlock and the base layer. Figure 9 shows that the average LTE for three of the sections is similar and varies from 88 to 95 percent (Good LTE), while LTE for Section 3019 is 76 percent (Fair LTE). Smaller LTE indicates less constraints from joints, thus allowing the slabs to more freely curl upward. This may be one of the contributing factors to Section 3019's highest upward curvature compared to other three sections. *On the other hand, one should note that the large upward curvature of the slabs on Section 3019 might have resulted in the low LTE values depending on the location of testing*.

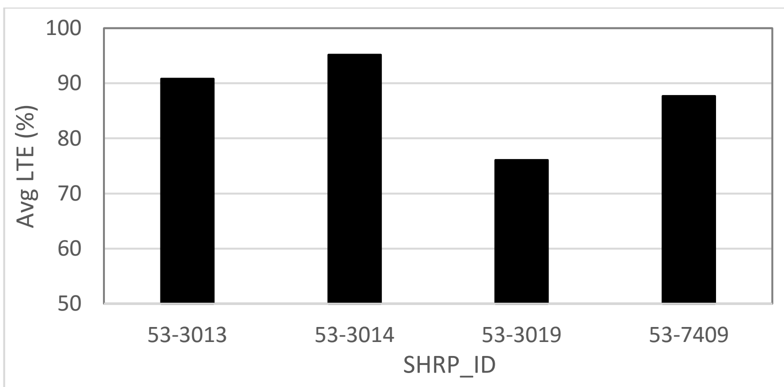

Figure 9 Comparison of Average LTE for the Four Sections

Construction Conditions. Exact TZ and the slab temperature profiles at TZ are required to quantify the $\Delta T_{built\text{-}in}$, however, these data are not available for the sections. Thus, temperature at TZ (T_z), used in the MEPDG as the trigger temperature for the slab to curl upward and develop tensile stresses was used to gain an understanding of construction conditions. Simply put, higher T_z results in larger $\Delta T_{built\text{-}in}$. The empirical equation used in the MEPDG for T_z is shown in Equation 3 (ARA 2004). As seen in Equation 3, T_z depends on the PCC mix design, cement content, and the mean monthly temperature (MMT) for the month of construction. The former two were available for each section as reposted in Table 4, and the latter was extracted from "MERRA" climatic database in the LTPP climatic database. However, Section 3019's temperature data was obtained from the National Oceanic and Atmospheric Administration (NOAA) because the climatic data in "MERRA" for this section was unavailable for the construction month. The estimated T_z for each section is shown in Figure 10.

$$T_z = (CC \cdot 0.59328 \cdot H \cdot 1000 \cdot 1.8/(1.1 \cdot 2400) + MMT) \qquad \text{Eq.3}$$

where,

T_z = temperature at TZ, °F.
CC = cementitious content, lb/yd^3.
H = -0.0787+0.007*MMT-0.00003*MMT^2
MMT = mean monthly temperature for month of construction, °F.

It can be seen that T_z for Sections 3013, 3014, and 3019 are similar at about 24°C (75.2°F), which are 5°C (9°F) higher than the one for Section 7409. It can be speculated that this difference in T_z is the reason why the EBITDs of Section 7409, which range from +31 to -28°C (+55 to -51°F), are lower than the other sections that range from -40 to -120°C (-72 to -215°F). The positive EBITDs of Section 7409 might be due to a late construction time, seeing that negative $\Delta T_{built\text{-}in}$ usually develops for morning construction and positive $\Delta T_{built\text{-}in}$ generates for late time construction. However, the comparison of T_z cannot explain why the negative EBITD of Section 3019 is higher than Section 3013 and 3014 since they have similar EBITDs. This can be explained by drying shrinkage effect.

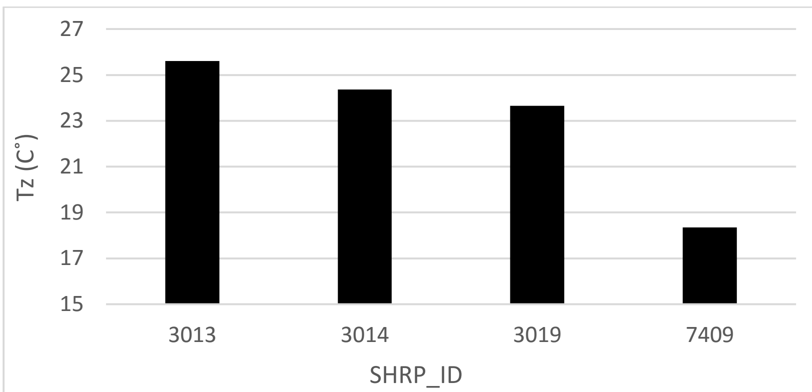

Figure 10. Comparison of T_Z for the Four Sections

Climatic Conditions All four sections are located in eastern Washington State, which is a dry climatic region, therefore drying shrinkage plays an important role in the development of negative EBITD in PCC pavements. Also, PCC mixture design, especially the water to cementitious materials ratios (w/cm) influences the ultimate drying shrinkage. From Table 2, Sections 3014 and 3019 have the lower w/cm values (0.33 and 0.34), resulting in less drying shrinkage than the other two sections with w/cm = 0.44 and 0.43), assuming similar environmental conditions. However, the sections are exposed to different environmental conditions. The annual average relative humidity (RH), extracted from “MERRA”, are shown in Figure 10 (a). Sections 3014 and 3019 are located in the driest climatic conditions. For more information, the difference between the annual average surface evaporation and surface precipitation (ΔEP) for the sections were collected from MERRA and are compared in Figure 10 (b). Section 3019 with the largest EBITD has the highest ΔEP (255 mm) compared to the other three sections. Also, note the falling trend in upward curvature for the three sections with the increase in ΔEP. To consider the effect of seasonal drying shrinkage, the average RH for the test month for each section is shown in Figure 10 (c). Compared to annual RH, the values of Section 3013 falls 33 percent and the other sections decrease around 14 percent, indicating that part of drying shrinkage was seasonal.

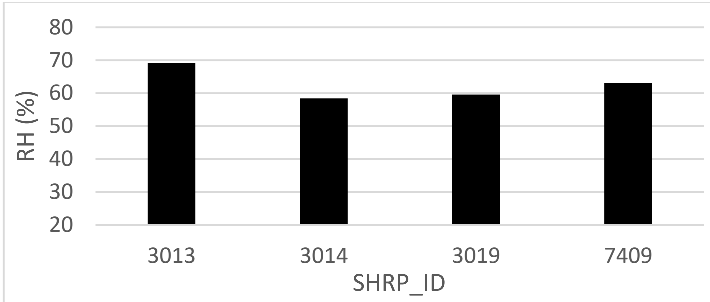

(a)

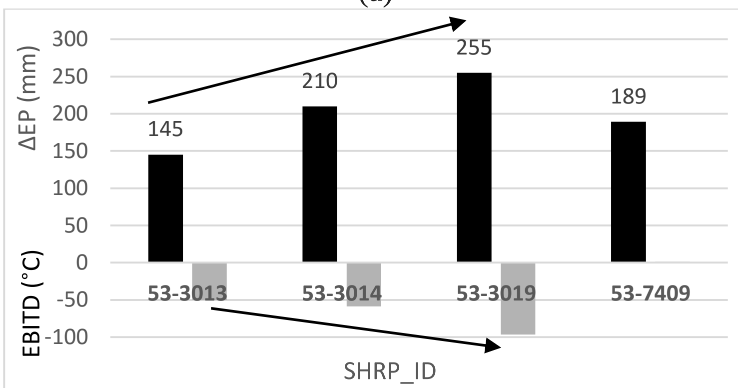

(b)

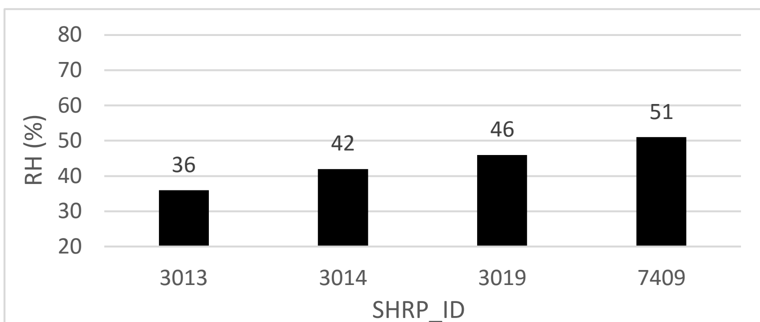

(c)

Figure 10. Comparison of (a) Annual Average RH, (b) Annual Average ΔEP, (c) Test Month Average RH.

Effect of Creep. The factors that contribute to creep relaxation in PCC slabs are mainly related to the slab weight, restraints at joints, and the friction between PCC and base layer. As discussed previously all sections had similar base layers. As discussed previously, Section 3019 had Fair LTE conditions, which can result in less creep compared to other sections with Good LTE. Further, creep is time-dependent, therefore the age of the sections (shown in Figure 11) influence the level of creep realized by the sections. Section 3013 is the oldest section and thereby more prone to the effects of creep relaxation. This contributes to explain that Section 3013 has lower negative EBITDs than Sections 3014 and 3019. However, Section 7409, which has smallest curvatures and is older than Sections 3014 and 3019, is younger than Section 3013. This behavior was speculated to be mainly due to the positive $\Delta T_{built\text{-}in}$ of this section as discussed before.

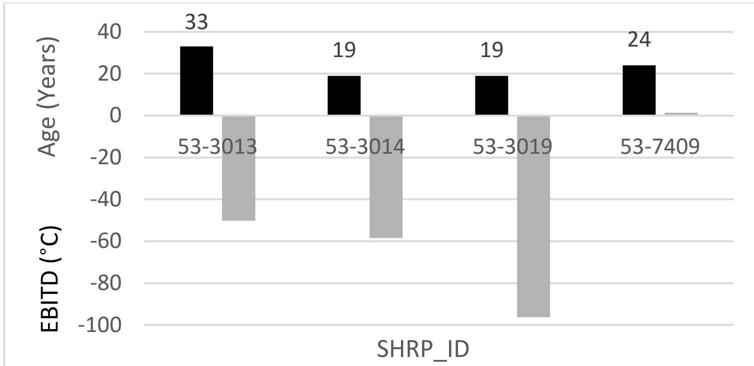

Figure 11. Comparison of Age for the Four Sections

Conclusions

Curling and warping of JPCPs are mainly due to ΔT_{tran}, $\Delta T_{built\text{-}in}$, shrinkage, and creep. EBITD, which represents the combined effects of $\Delta T_{built\text{-}in}$, shrinkage, and creep, was established in this study for four JPCP sections in the LTPP program. ISLAB2000 was used to find the TBITDs for fifteen PCC slabs in four JPCP sections located in eastern Washington State through matching the predicted and measured mid-slab deflection (δ_{mid}) and slab curvature (ε_{trans}). Then, the EBITDs were quantified by subtracting ΔT_{tran} from the TBITDs.

It was found that large negative EBITDs developed in Sections 3013, 3014, and 3019, with Section 3019 showing the largest upward curvature. Section 7409 showed small values of both positive and negative EBITDs (close to a relatively flat condition).

Section 3019, which developed the largest negative EBITDs, turned out to have lowest LTEs. The comparison of T_z indicate that the $\Delta T_{built\text{-}in}$ of Section 3013, 3014, and 3019 were potentially similar and larger than Section 7409, which has the smallest upward curvature. The small positive EBITDs in Section 7409 was hypothesized to be related to the construction time. The comparisons of annual relative humidity (RH) and the difference between the annual average surface evaporation and surface precipitation (ΔEP) for the sections suggest that Section 3019 followed by Section 3014 see the most drying shrinkage effect, explaining the large upward curvature in Section 3019. At last, the effect of creep was considered. Sections 3013 and 7409 are older than the other two sections, with higher expected creep effect. This helps explain why the EBITDs were lower in these two sections. However, the fact that Section 7409 has lowest EBITDs but is not the oldest section needs to be explained together with its less drying shrinkage and small $\Delta T_{built\text{-}in}$ as discussed previously.

Except for the surface restoration and dowel bar retrofit activities on Sections 3013 and 7409, no other major rehabilitation activity has been performed on the sections. Three of the sections are in good conditions, while Section 7409 shows low- and medium-severity fatigue cracking. The possibly large $\Delta T_{built\text{-}in}$ maybe the cause of fatigue cracking in this section.

References

AASHTO. (1993). *AASHTO Guide for Design of Pavement Structures 1993*, American Association of State Highway and Transportation Officials, Washington, DC.

Armaghani, J.M., Larsen, T.J., and Smith, L.L. (1987). "Temperature response of concrete pavements." *Transportation Research Record*, Transportation Research Board, Washington DC, 1121, 23-33.

ARA, Inc., ERES Division. (2004). *Guide for Mechanistic – Empirical Design of New and Rehabilitated Pavement Structure. Final Report NCHRP 1-37A.*

Burnham, T., and Koubaa, A. (2001). "A new approach to estimate the in-situ thermal coefficient and drying shrinkage for jointed concrete pavement." *Proc., 7th International Conference on Concrete Pavements*, International Society for Concrete Pavements, Orlando, Florida, 313-332.

Eisenmann, J., and Leykauf, G. (1990). "Effects of paving temperatures on pavement performance." *Proc., 2nd International Workshop on Theoretical Design of Concrete Pavements,* Madrid, Spain, 419-428.

Eisenmann, J., and Leykauf, G. (1990). "Simplified calculation method of slab curling caused by surface shrinkage." *Proc, 2nd International Workshop on Theoretical Design of Concrete Pavements. Madrid, Spain*.

Janssen, D. J. (1987). "Moisture in Portland cement concrete." *Transportation Research Record*, Transportation Research Board, Washington, DC, 1121, 40-44.

Janssen, D. J., and Snyder, M. B. (2000). "Temperature-moment concept for evaluating pavement temperature Data." *Journal of infrastructure systems*, 6(2), 81-83.

Khazanovich, L., Tayabji, S. D., and Darter, M. I. (2001). *Backcalculation of layer parameters for LTPP test sections, Volume 1: slab on elastic solid and slab on dense-liquid foundation analysis of rigid pavements*. Federal Highway Administration, McLean, Virginia.

Kim, S., Gopalakrishnan, K., and Ceylan, H. (2011). "A simplified approach for predicting early-age concrete pavement deformation." *Journal of Civil Engineering and Management*, 17(1), 27-35.

Nassiri, S., and Vandenbossche, J. M. (2012). "Establishing built-in temperature gradient for jointed plain concrete pavements in Pennsylvania". *International Journal of Pavement Research and Technology*, *5*(4), 245.

Nassiri, S., Vandenbossche, J., and Janssen, D. (2014). "Methodology for identifying zero-stress time for jointed plain concrete pavements." *Transportation Research Record: Journal of the Transportation Research Board*, 2441, 62-71.

Rao, C., Barenberg, E. J., Snyder, M. B., and Schmidt, S. (2001). "Effects of temperature and moisture on the response of jointed concrete pavements." *Proc., 7th International Conference on Concrete Pavements. The Use of Concrete in Developing Long-Lasting Pavement Solutions for the 21st Century*, International Society for Concrete Pavements, Orlando, Florida, 23-38.

Rao, S., and Roesler, J. R. (2005). "Characterizing effective built-in curling from concrete pavement field measurements." *Journal of Transportation Engineering*, 131(4), 320-327.

Rao, C., Titus-Glover, L., Bhattacharya, B. B., and Darter, M. I. (2011). "Estimation of deltaT input for JPCP design using the MEPDG." *Proc. Transportation Research Board 90th Annual Meeting*, Transportation Research Board, Washington, DC, No. 11-3938.

Schmalzer, P. N. (2006). *Long-term pavement performance program manual for falling weight deflectometer measurements*, Federal Highway Administration, Office of Research, Development and Technology, Turner-Fairbank Highway Research Center, McLean, Virginia.

Westergaard, H. M. (1927). "Analysis of stresses in concrete pavements due to variations of temperature." *Proc., Sixth Annual Meeting of the Highway Research Board*, Highway Research Board, Washington, DC, Vol.6, 201-215.

Yu, H., Khazanovich, L., Darter, M., and Ardani, A. (1998). "Analysis of concrete pavement responses to temperature and wheel loads measured from instrumented slabs." *Transportation Research Record: Journal of the Transportation Research Board*, 1639, 94-101.

Yu, H. T., Khazanovich, L., and Darter, M. I. (2004). "Consideration of JPCP curling and warping in the 2002 design guide". *Proc., 83rd Annual Meeting of the Transportation Research Board* (CD-Rom), Transportation Research Board, Washington, DC.